Modified Bounding Surface Hypoplasticity Model for Sands under Cyclic Loading

Gang Wang, M.ASCE[1]; and Yongning Xie[2]

Abstract: A modified bounding surface hypoplasticity model is developed to capture distinct dilatancy behaviors of loose and dense sandy soils during various phases of undrained cyclic loading. Based on observations from laboratory tests, new modulus formulations are proposed to improve the simulation of cyclic mobility and postliquefaction behaviors of both loose and dense sands. The state-dependent dilatancy and effects of accumulated plastic strains on the plastic moduli are also incorporated in this model. The model demonstrates excellent capabilities through systematic comparison between the model predictions and a series of undrained cyclic simple shear tests on Fraser River sand.
DOI: 10.1061/(ASCE)EM.1943-7889.0000654.

Author keywords: Constitutive model; Bounding surface hypoplasticity; Liquefaction; Cyclic response.

Introduction

Realistic simulation of liquefaction in granular soils is one of the major challenges in constitutive modeling of geomaterials. Following the terminology introduced in Kramer (1996), liquefaction refers to a range of phenomena that can be divided into two main groups: flow liquefaction and cyclic mobility. Under static or cyclic loading, granular soils exhibit the tendency for densification, which causes an increase in excess pore pressures and decrease in effective stresses under a saturated and undrained condition. Flow liquefaction often occurs in very loose sands when the shear stress is greater than the shear strength of the liquefied soils. It is characterized by a sudden loss of the soil strength and is often associated with large deformations and a flow-type failure. The flow slide failure of the Lower San Fernando Dam during the 1971 San Fernando Earthquake is such an example. On the other hand, cyclic mobility occurs when the cyclic shear stress is less than the shear strength of the liquefied soil. Cyclic mobility can occur in a much broader range of soils and site conditions than flow liquefaction. It is characterized by progressive accumulation of shear deformations under cyclic loading and has the potential to result in unacceptably large permanent displacements. Both flow liquefaction and cyclic mobility can cause severe damages to civil structures during earthquakes, including overturning of buildings on liquefied ground caused by loss of bearing capacity, flow failure of earth structures, large lateral spreading of the liquefied ground, and excessive postliquefaction settlements.

Significant progress has been made in the last 30 years to simulate the fundamental stress-strain-strength relationships of granular soils under static and cyclic loading conditions (Prevost 1981; Dafalias 1986; Wang et al. 1990; Pastor et al. 1990; Manzari and Dafalias 1997; Zienkiewicz et al. 1999; Li 2002; Elgamal et al. 2003; Yang et al. 2003; Park and Byrne 2004; Dafalias and Manzari 2004; Taiebat and Dafalias 2008; Anandarajah 2008; Yin et al. 2010; Yin and Chang 2013). Among them, the bounding surface model by Wang et al. (1990) has been successfully developed to simulate a fully nonlinear site response (Li et al. 1992, 1998; Arulanandan et al. 2000; Wang et al. 2001) and earthquake-induced liquefaction and deformation of earth structures (Wang and Makdisi 1999; Wang et al. 2006). However, the original Wang et al. (1990) model suffers several limitations. The model does not prescribe a zero dilatancy at the limit of critical state. Therefore, it is not consistent with the critical state theory and cannot properly characterize the stress-strain-strength behaviors at the liquefied state. The original model was developed using available test data on (liquefiable) loose sands. Although it can simulate the cyclic response of loose sands reasonably well, it cannot accurately capture the dilatancy behaviors and the cyclic response of dense sands.

To overcome these difficulties, a modified bounding surface hypoplasticity model based on the original framework of Wang et al. (1990) is developed in this study. As the volumetric dilatancy is closely related to the pore pressure generation and effective stress path under undrained cyclic loading, it is one of the key components in constitutive modeling. This study proposes new modulus formulations to describe the distinct dilatancy behaviors of loose and dense sands during various phases of cyclic loading based on observation from laboratory tests. The model also incorporates a state-dependent dilatancy surface and considers the influence of accumulated plastic strains on plastic moduli to improve the simulation of cyclic mobility and postliquefaction behaviors. The detailed model formulation will be presented in the following sections. Systematic comparison between the model predictions and experimental test results will be conducted to demonstrate the excellent model capabilities.

Modified Model Formulation

In this section, the modified bounding surface plasticity model is presented. Throughout the paper, bold symbols indicate tensors or vectors, and a superposed dot denotes the rate of a tensor. Tensor operations follow the convention of summation over repeated indexes, $\mathbf{a} \otimes \mathbf{b} = a_{ij}b_{kl}$, $\mathbf{a}:\mathbf{b} = a_{ij}b_{ji}$, and $tr(\mathbf{a}) = a_{ii}$. Unless otherwise

[1]Assistant Professor, Dept. of Civil and Environmental Engineering, Hong Kong Univ. of Science and Technology, Clear Water Bay, Kowloon, Hong Kong (corresponding author). E-mail: gwang@ust.hk

[2]Graduate Student, Dept. of Civil and Environmental Engineering, Hong Kong Univ. of Science and Technology, Clear Water Bay, Kowloon, Hong Kong.

Note. This manuscript was submitted on July 2, 2012; approved on April 3, 2013; published online on April 5, 2013. Discussion period open until June 1, 2014; separate discussions must be submitted for individual papers. This paper is part of the ***Journal of Engineering Mechanics***, Vol. 140, No. 1, January 1, 2014. ©ASCE, ISSN 0733-9399/2014/1-91–101/$25.00.

stated, all stress tensors refer to effective stress quantities. Sign convention assumes that compressive strain and stress are positive.

Bounding Surface and Mapping Rules

Following Wang et al. (1990), the effective stress rate is decomposed as

$$\dot{\boldsymbol{\sigma}} = p\dot{\mathbf{r}} + \dot{p}\frac{\boldsymbol{\sigma}}{p} = p\dot{\mathbf{r}} + (\mathbf{r} + \mathbf{I})\dot{p} \tag{1}$$

where $\boldsymbol{\sigma}$ = effective stress tensor; and $p = 1/3tr(\boldsymbol{\sigma})$ = effective mean stress. The deviatoric stress ratio tensor is defined as $\mathbf{r} = \mathbf{s}/p$, $\mathbf{s} = \boldsymbol{\sigma} - p\mathbf{I}$ is the deviatoric stress tensor, and $\mathbf{I}$ is the second-order identity tensor. This decomposition resolves the stress rate into $p\dot{\mathbf{r}}$ and $\dot{p}$, which is different from the classical $\dot{\boldsymbol{\sigma}} = \dot{\mathbf{s}} + \dot{p}\mathbf{I}$ decomposition.

The stress ratio invariant, defined as $R = \sqrt{1/2\,\mathbf{r}:\mathbf{r}}$, will be used to define the following three bounding surfaces:

1. The failure surface, $R - R_f = 0$, specifies the ultimate limit of an admissible stress ratio invariant R. The value of R_f is related to intrinsic properties of the soil (e.g., frictional angle), and it is usually assumed to be a constant value.
2. The maximum prestress surface, $R - R_m = 0$, defines the maximum stress ratio that was experienced by the material. R_m is a record of the maximum past history, and it will be updated only if the current R exceeds this value.
3. The dilatancy surface, $R - R_p = 0$, defines the location where transformation from contractive to dilative behavior occurs. These three bounding surfaces can be plotted in the $p - J$ space (where J is an isotropic invariant, $J = \sqrt{1/2\,\mathbf{s}:\mathbf{s}} = pR$) in Fig. 1(a). The failure surface and the maximum prestress surface are shown as straight lines if R_f and R_m values are given. On the other hand, the dilatancy line is a curved line in the $p - J$ space. The dilatancy line is closely related to the volumetric behaviors of granular soils, and it will be discussed in detail in the next section.

To simplify the presentation, the bounding surfaces assume conical shapes in a three-dimensional principal stress space in Fig. 1(b). The bounding surfaces is circular when plotted in the stress ratio space in Fig. 1(c). In this plot, the current stress state is represented by vector $\mathbf{r}$. A projection center $\boldsymbol{\alpha}$ is defined as the last stress reversal point in reverse unloading or is set to the origin if the current stress state exceeds the maximum prestress surface R_m in virgin loading. An image stress point $\bar{\mathbf{r}}$ is defined as the point projected on the R_m surface from the projection center $\boldsymbol{\alpha}$ through the current stress state point $\mathbf{r}$. The class of bounding surface hypoplasticity models usually postulates nonlinear stress-strain relationships through smooth interpolation between the current stress point and the image stress point. For this purpose, the scalar quantities ρ and $\bar{\rho}$ measure the distances between $\boldsymbol{\alpha}$, $\mathbf{r}$, and $\bar{\mathbf{r}}$, and their ratio $\bar{\rho}/\rho$ will be used in the plastic modulus formulation to capture the nonlinear stress strain behavior during the loading-unloading-reloading process. Under a monotonic loading path, the projection center will remain at the origin and $\rho = \bar{\rho}$. At the moment of cyclic unloading, the current stress point coincides with the stress reverse point so that $\rho = 0$.

It is also worth mentioning that an increase in the mean effective stress may induce volumetric plastic strain partially because of particle crushing, which can be readily considered by introducing a flat cap model or an enclosed yield surface as proposed in Wang et al. (1990) and Taiebat and Dafalias (2008). However, the pressure-induced plastic volumetric change can be neglected for most practical purposes. It has been observed that the mean effective

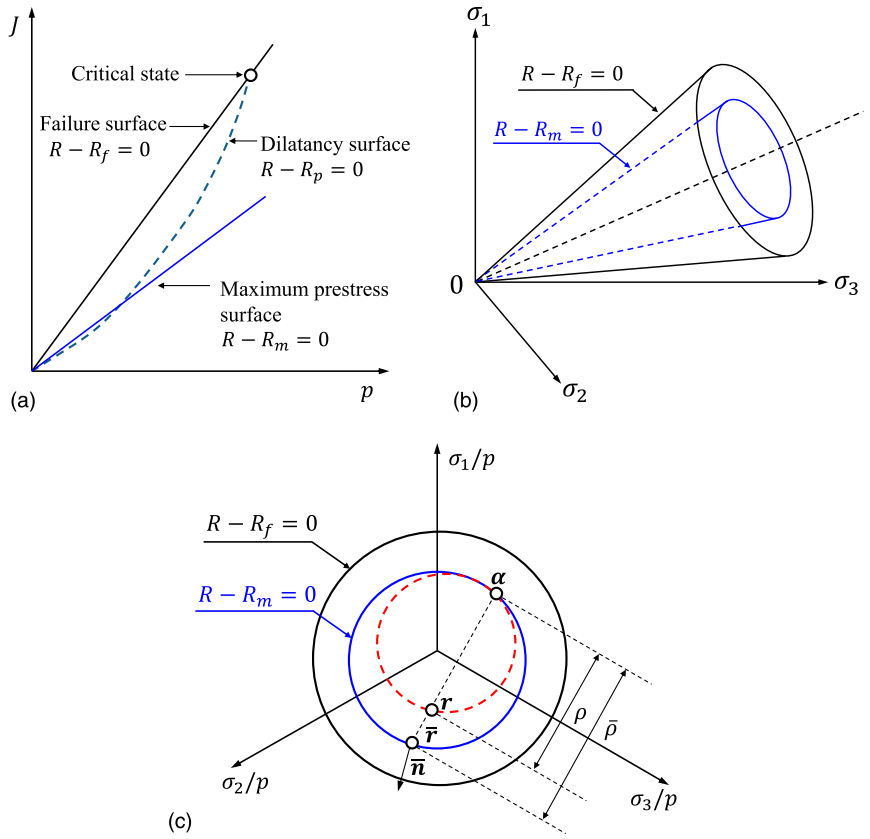

Fig. 1. Definition of bounding surfaces

J. Eng. Mech. 2014.140:91-101.

stress usually decreases during undrained cyclic loading. Besides, the plastic volumetric strains are usually negligible under the range of mean effective stress of engineering interest (Manzari and Dafalias 1997; Li et al. 1999). In this paper, an open conical failure surface is assumed for simplicity, as shown in Fig. 1(b).

Dilatancy Line

Under undrained cyclic loading, change in the effective stress is associated with shear-induced volumetric dilative or contractive tendency of the soil. The dilatancy line $R - R_p = 0$ specifies the location where a contractive phase transforms to a dilative phase, and it is one of the most critical components to describe the cyclic behaviors of granular soils. If the stress state is on the dilatancy line ($R = R_p$), the soil will exhibit zero volumetric dilatancy (i.e., no volumetric change). As pointed out by Manzari and Dafalias (1997), a constant R_p will result in unrealistic nonzero dilation at failure. They concluded that R_p must be a variable, and the dilatancy line must pass through the critical state point to be consistent with the critical state concept, which states that there is no volume change at failure. One approach is to postulate that R_p is dependent on state variables. The so-called state-dependent dilatancy (Li et al. 1999) assumes that R_p follows the following relationship:

$$R_p = R_f e^{m\psi} \tag{2}$$

where ψ = state parameter defined as the difference between the current void ratio e and the critical void ratio e_c associated with the current mean effective stress p, i.e., $\psi = e - e_c$ (Been and Jefferies 1985). Alternative state variables were also proposed for the same purpose (Wang and Makdisi 1999; Wang et al. 2002). The critical state line of Fraser River sand is illustrated in Fig. 2. The critical void ratio e_c is related to p through the following equation (Li and Wang 1998):

$$e_c = e_\Gamma - \lambda \left(\frac{p}{p_a}\right)^{\xi} \tag{3}$$

where e_Γ, λ, and ξ = critical state parameters that can be obtained from undrained triaxial tests (Verdugo and Ishihara 1996). By

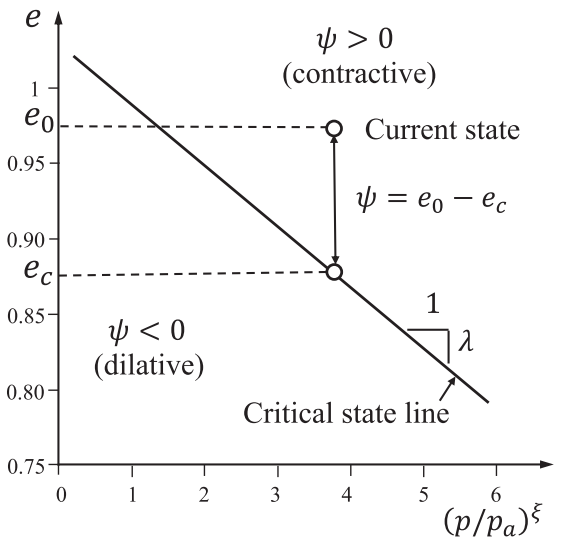

Fig. 2. Definition of state parameter

combining Eqs. (2) and (3), the dilatancy line can be mathematically defined as

$$J = pR_f \exp\left\{m\left[e - e_\Gamma + \lambda (p/p_a)^{\xi}\right]\right\} \tag{4}$$

Following Li and Wang (1998), $\xi = 0.7$ is adopted in this study. The concept of state-dependent dilatancy is consistent with the critical state theory. When the soil approaches its critical state ($R \to R_f$), the state parameter ψ approaches zero. Therefore, the phase transformation point R_p coincides with the failure point R_f, prescribing a zero dilatancy at the critical state limit. Under undrained conditions, the void ratio remains constant. Therefore, the dilatancy line is represented in Figs. 1 and 3 by a curve through the critical state using Eq. (4).

The parameter m is a nonnegative model parameter. By examining the laboratory test data, a constant value cannot be assigned to m to realistically represent the dilatancy lines of both loose and dense samples. In Fig. 3, $m = 4$ and 1.2 is used for dense ($D_r = 80\%$) and relatively loose ($D_r = 40\%$) samples, respectively. The soil is contractive if its stress state is below the dilatancy line, and dilative if its stress state is above the line. The dilatancy line starts from the origin and curves up toward the critical state point (labeled as C_1 and C_2 in Fig. 3) on the failure line. By comparison, the dilatancy line of the loose sample is much closer to the failure line, indicating it is more contractive than the dense sample. However, for the range of mean effective stress of engineering interest (0−300 kPa shown in the inset of Fig. 3), the dilatancy line can be approximated by a straight line. In this example, R_p/R_f is approximately 0.89 and 0.34 for loose and dense samples, respectively.

Stress-Strain Relationship

The elastic strain can be decomposed into a deviatoric and a volumetric part. Accordingly, the elastic stress-strain relationship can be written as

$$\dot{\boldsymbol{\varepsilon}}^e = \dot{\mathbf{e}}^e + \frac{1}{3}(tr\dot{\boldsymbol{\varepsilon}}^e)\mathbf{I} = \frac{1}{2G}\dot{\mathbf{s}} + \frac{1}{3}\dot{p}\mathbf{I} = \frac{1}{2G}p\dot{\mathbf{r}} + \left(\frac{1}{2G}\mathbf{r} + \frac{1}{3K}\mathbf{I}\right)\dot{p} \tag{5}$$

where G and K = elastic shear and bulk moduli, respectively.

Following the framework and basic formulations set forth by Wang (1990) and Wang et al. (1990), the plastic strain increment is

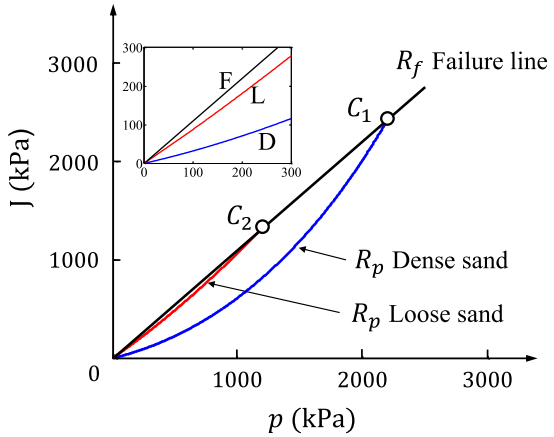

Fig. 3. Dilatancy line (inset: F = failure line; L = loose sand dilatancy line; D = dense sand dilatancy line)

J. Eng. Mech. 2014.140:91-101.

decomposed into two mechanisms associated with the stress components $p\dot{\mathbf{r}}$ and $\dot{p}$

$$\dot{\boldsymbol{\varepsilon}}^{\boldsymbol{p}} = \left(\frac{1}{H_r}\overline{\mathbf{n}} + \frac{1}{3K_r}\mathbf{I}\right)(p\dot{\mathbf{r}}:\overline{\mathbf{n}}) + \left(\frac{1}{H_p}\mathbf{r} + \frac{1}{3K_p}\mathbf{I}\right)h(p-p_m)\langle\dot{p}\rangle \quad (6)$$

where H_r and K_r = plastic shear and bulk moduli associated with the deviatoric and volumetric plastic strains induced by $p\dot{\mathbf{r}}$, respectively; and H_p and K_p = corresponding plastic shear and bulk moduli associated with $\dot{p}$, respectively. The $\overline{\mathbf{n}}$ is a deviatoric unit tensor specifying the direction of the deviatoric plastic strain rate, which is defined as normal to the maximum prestress surface at the image point $\overline{\mathbf{r}}$. The $p\dot{\mathbf{r}}:\overline{\mathbf{n}}$ is the so-called loading index, a scalar quantity that controls the extent of the plastic strain rate. The heaviside step function $h(p-p_m)$ and the Macaulay brackets $\langle\rangle$ indicate the plastic strain associated with $\dot{p}$ operates only if the present p exceeds the past maximum mean effective stress, p_m and increases ($\dot{p}>0$). It can be regarded as a cap model. As discussed previously, the second part in Eq. (6) can be neglected for most practical purposes. Therefore, Eq. (6) can be simplified as

$$\dot{\boldsymbol{\varepsilon}}^{\boldsymbol{p}} = \left(\frac{1}{H_r}\overline{\mathbf{n}} + \frac{1}{3K_r}\mathbf{I}\right)(p\dot{\mathbf{r}}:\overline{\mathbf{n}}) \quad (7)$$

The dilatancy of materials can be obtained as follows (Li et al. 1999):

$$d = \frac{\dot{\varepsilon}_v^p}{\dot{\varepsilon}_q^p} = \frac{\dot{\varepsilon}_v^p}{\sqrt{\frac{2}{3}\dot{\mathbf{e}}^p:\dot{\mathbf{e}}^p}} = \sqrt{\frac{3}{2}}\frac{H_r}{K_r} \quad (8)$$

where $\dot{\varepsilon}_v^p$ and $\dot{\varepsilon}_q^p$ = plastic volumetric strain rate and equivalent plastic shear strain rate, respectively; and $\dot{\varepsilon}_q^p = \sqrt{(2/3)\dot{\mathbf{e}}^p:\dot{\mathbf{e}}^p}$, where $\dot{\mathbf{e}}^p$ = plastic deviatoric strain rate.

Combining Eqs. (5) and (7), the effective stress rate $\dot{\boldsymbol{\sigma}}$ is related to the strain rate $\dot{\boldsymbol{\varepsilon}}$ via an elastoplastic modulus $\mathbf{D}^{ep}$ (Wang et al. 1990)

$$\dot{\boldsymbol{\sigma}} = \mathbf{D}^{ep}:\dot{\boldsymbol{\varepsilon}} \quad (9)$$

where

$$\mathbf{D}^{ep} = \mathbf{D}^{e} - \frac{\mathbf{p}^r \otimes \mathbf{Q}^p}{A_r B_p - A_p B_r} \quad (10)$$

and

$$D^e_{ijkl} = K\delta_{ij}\delta_{kl} + G\left(\delta_{ik}\delta_{jl} + \delta_{il}\delta_{jk} - \frac{2}{3}\delta_{ij}\delta_{kl}\right) \quad (11)$$

$$\mathbf{p}^r = \frac{2G}{H_r}\overline{\mathbf{n}} + \frac{K}{K_r}\mathbf{I} \quad (12)$$

$$\mathbf{Q}^p = B_p\overline{\mathbf{n}} - B_r\mathbf{I} \quad (13)$$

$$A_r = \frac{1}{2G} + \frac{1}{H_r}; \quad A_p = \frac{1}{K_r} \quad (14)$$

$$B_r = \frac{1}{2G}\mathbf{r}:\overline{\mathbf{n}}; \quad B_p = \frac{1}{K} \quad (15)$$

Detailed formulations for the elastic moduli G and K, and plastic moduli H_r and K_r are presented in the next section.

Elastic and Plastic Moduli Formulation

The elastic shear and bulk moduli G and K are given by the following empirical equations (Wang et al. 1990):

$$G = p_a G_0 \frac{(2.973-e)^2}{1+e}\left(\frac{p}{p_a}\right)^{1/2} \quad (16)$$

$$K = p_a \frac{1+e}{\kappa}\left(\frac{p}{p_a}\right)^{1/2} \quad (17)$$

where p = current mean effective stress; p_a = atmospheric pressure; G_0 = modulus coefficient related to the small-strain shear modulus; e = current void ratio; and κ = slope of an unloading-reloading path of isotropic consolidation tests in e versus the $2\sqrt{p/p_a}$ plot (Li et al. 1999). The elastic shear and bulk moduli can also be related to Poisson's ratio ν

$$K = \frac{2G(1+\nu)}{3(1-2\nu)} \quad (18)$$

Therefore, κ and ν are not independent variables. Combining Eqs. (16)–(18) leads to the following relationship between κ and ν:

$$\kappa = \frac{3(1-2\nu)}{2G_0(1+\nu)}\left(\frac{1+e}{2.973-e}\right)^2 \quad (19)$$

The plastic moduli are related to the elastic moduli by introducing additional terms to account for nonlinear behaviors. The plastic shear modulus H_r is modified from Wang et al. (1990) and is defined as follows:

$$H_r = Gh_r C_H(\xi_q)\left[\frac{R_f}{R_m}\left(\frac{\overline{\rho}}{\rho}\right)^{m'} - 1\right]\left(\frac{p}{p_m}\right)^{1/2} \quad (20)$$

where

$$C_H(\xi_q) = \frac{1}{1+\alpha\xi_q}; \quad \xi_q = \int_0^{\mathbf{e}^p}\sqrt{\frac{2}{3}d\mathbf{e}^p:d\mathbf{e}^p} \quad (21)$$

$$m' = 2R_m/\overline{\rho} \quad (22)$$

where h_r = dimensionless material constant. Some previous studies also associate it with the void ratio (Li et al. 1999; Wang et al. 2002; Dafalias and Manzari 2004). $C_H(\xi_q)$ is incorporated to account for the influence of accumulated deviatoric plastic strain, ξ_q, on the plastic modulus ($d\mathbf{e}^p$ is the deviatoric plastic strain increment). Parameter α is used to control the extent of the strain dependence. The strain-dependent term is essential to effectively represent the cyclic mobility (Wang and Dafalias 2002). Without the strain-dependent term, a stabilized cyclic stress-strain curve will eventually be reached under a repeated cyclic loading if the constitutive model is formulated solely in the stress space. It is also noted that an additional pressure-dependent term $(p/p_m)^{1/2}$ is introduced in this study to strengthen the influence of the mean effective stress on the plastic shear modulus. The term can effectively improve the postliquefaction stress-strain hysteresis behaviors. By comparison, modulus formulation without this pressure term usually yields a much fatter cyclic stress-strain loop and an overestimated hysteretic damping if a damping correction scheme is not applied (Wang et al. 2008).

The plastic bulk modulus K_r is formulated by modifying the elastic bulk modulus K as follows:

$$K_r = p_a \frac{1+e_{in}}{w\kappa}\left(\frac{p}{p_a}\right)^{1/2} = \frac{K}{w} \tag{23}$$

The original formulation for w assumes the following form (Wang et al. 1990):

$$w = \begin{cases} w_m = \dfrac{1}{k_r' C(\xi)'}\left(\dfrac{p}{p_m}\right)^{a'}\left(\dfrac{R_m}{R_f}\right)^{b'}\left(\dfrac{R_p - R_m}{R_f - R_m}\right), & \text{if } R = R_m \\ w_r = \dfrac{1}{C(\xi)'}\left(\dfrac{R_m}{R_f}\right)^{d'}, & \text{otherwise} \end{cases} \tag{24}$$

where $C(\xi)'$ = strain-dependent term; and a', b', and d' = constant parameters. This formulation distinguishes dilatancy behavior during a virgin loading and reverse loading. In the virgin loading (i.e., $R = R_m$), the soil dilatancy is prescribed by w_m such that dilation occurs only if the dilatancy line is exceeded ($R_m > R_p$, and $w = w_m$ is negative). During the subsequent reverse loading, a positive w_r is assumed, which always prescribes a contractive behavior. Additional dilation occurs only if the maximum prestress R_m is exceeded and a negative $w = w_m$ is invoked.

It is worth pointing out that the previous postulate works reasonably well for loose sands and cases with a higher dilatancy line (e.g., $R_p > 0.75R_f$); however, it cannot be used to realistically simulate the strong dilative behaviors of the dense sands. The operation of the original formulation is schematically illustrated in Fig. 5. Following a cyclic stress path starting from Point (1), w_m is used for the virgin Loading Path (1) to (3). The soil is contractive from (1) to (2) (i.e., $w_m > 0$), followed by a dilative phase from (2) to (3) (i.e., $w_m < 0$), and $w_m = 0$ at the phase Transformation Point (2). The maximum prestress is set as $R_m^{(1)}$ at the Stress Reversal Point (3). Reverse loading from (3) to (5) is contractive because $R < R_m^{(1)}$ and $w_r > 0$. The phase transformation point at (4) will be simply crossed over with no occurrence of phase transformation. The actual phase transformation from contractive to dilative behavior takes place at Point (5), where the maximum prestress $R_m^{(1)}$ is exceeded and a negative w_m is invoked. Similar behaviors can be observed in the subsequent loading cycles, where phase transformation only occurs at an updated maximum prestress point rather than the prescribed phase transformation point. As the R_p line is close to the R_f line for loose sands, the original formulation still works reasonably well for this case. However, the original formulation fails to realistically simulate the strong dilative behaviors of the dense sand as the phase transformation cannot be effectively prescribed using the original formulation.

Laboratory tests reveal that the dilatancy line of dense sands is usually much lower (e.g., $R_p = 0.3R_f$) than loose sands, and it is not significantly affected by virgin loading. In this study, a more general formulation is proposed to describe the volumetric dilatancy for both dense and loose sands as follows:

$$w = \begin{cases} w_1 = \dfrac{1}{k_r}\left(\dfrac{R_m}{R_f}\right)^{b}\left(\dfrac{R_p - R}{R_f - R_m}\right), & \text{if } R = R_m \text{ or } R > R_p, \text{ and } \dot{R} > 0 \\ w_2 = C_K(\xi_v)\left(\dfrac{R_m + \text{sign}(\dot{R})R}{R_f}\right)\left(\dfrac{R_p - \text{sign}(\dot{R})R}{R_p + R_m}\right), & \text{otherwise} \end{cases} \tag{25}$$

and

$$C_K(\xi_v) = d_1 + d_2 \tanh(100\xi_v) \tag{26}$$

$$\xi_v = \int_0^{\varepsilon_v^p} \langle -d\varepsilon_v^p \rangle \tag{27}$$

This formulation is based on the following postulates: (1) the dilatancy line is not affected by virgin loading; (2) w_1 is used for the virgin loading ($R = R_m$ and $\dot{R} > 0$), or when R_p is exceeded in the reverse loading ($R > R_p$ and $\dot{R} > 0$); and (3) for all other cases, the soil always exhibits a contractive response, which is described by w_2 (always a nonnegative value). The operation of w during various phases of cyclic loading is illustrated in details in Fig. 4. Although the general formulation is proposed for both dense and loose soil samples, the operation is illustrated separately for each case for clarity. Fig. 4(a) shows the cyclic stress path of a dense sand. The soil is in the stage of virgin loading starting from (1) to (3), the maximum prestress surface coincides with the current stress state, i.e., $R = R_m$ and $\dot{R} > 0$. Therefore, $w = w_1$ is used, and it is a positive number implying a contractive response. The dilatancy line is reached at Point (2), $w_1 = 0$. Beyond that point, $w_1 > 0$, the soil transforms from a contractive to a dilative response. The maximum prestress R_m is updated to $R_m^{(1)}$ at Point (3). The condition for w_1 cannot be satisfied when the soil experiences reverse loading from Point (3) to Point (4). Therefore, $w = w_2$ is used, and the soil is contractive ($w_2 > 0$). From Point (4) to Point (5), the condition of $R > R_p$ and $\dot{R} > 0$ is met, so $w = w_1$ is invoked again and the soil is dilative during this phase. Consequently, the maximum prestress R_m is updated to $R_m^{(2)}$ at Point (5). The remaining loading path follows the same rules of operation as was described. As the effective stress reduces, the stress path exhibits a distinctive *butterfly* pattern in the

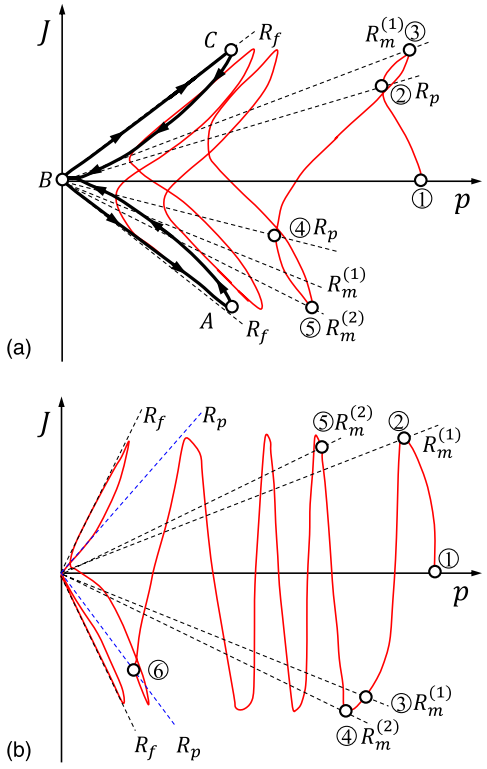

Fig. 4. Effective stress paths of dense and loose sands

J. Eng. Mech. 2014.140:91-101.

$p-J$ space, as shown with thicker solid lines (loop $A \rightarrow B \rightarrow C \rightarrow B \rightarrow A$) in Fig. 4(a). The stress path will essentially repeat the *butterfly* loop under continued loading cycles. Fig. 4(b).shows a representative cyclic stress path of a loose sand. For the loose sample, the dilatancy line R_p is in general close to the failure line. Before the stress path reaches the R_p line [Point (1) to Point (6)], $w = w_1$ is invoked when $R = R_m$ (virgin loading), while $w = w_2$ is used when $R < R_m$. The soil exhibits contractive behavior during the process. When R_p is reached at Point (6), it follows the same rule as was described for the dense case. From the previous description, it is noted that w_2 always assumes a nonnegative value and is used only for the contractive phases. w_1 is used for all dilative phases, but it can also be used prescribe a contractive response if $R = R_m$ (virgin loading) and $R < R_p$. The term $\{[R_m + \text{sign}(\dot{R})R]/R_f\}$ in Eq. (25) accounts for the influence of current stress state. It assumes a small nonnegative value of $[(R_m - R)/R_f]$ at the instance of unloading ($\dot{R} < 0$) and increases to $[(R_m + R_p)/R_f]$ on the dilatancy line. The term $\{[R_p - \text{sign}(\dot{R})R]/(R_p + R_m)\}$ varies from a value of $[(R_p + R)/(R_p + R_m) \leq 1]$ at the point of unloading to 0 at the point $R = R_p$.

Experiments (Ishihara et al. 1975) and micromechanical analysis (Nemat-Nasser and Tobita 1982) have revealed the effects of preceding dilative phases on the subsequent contractive phases. It was observed that the soil would experience a stronger contractive response following a dilative phase. This effect is modeled in this study by using $C_k(\xi_v)$ term in Eqs. (25) and (26), where parameter ξ_v is the plastic volumetric strain accumulated only during dilative phases. For this purpose, the Macaulay bracket $\langle\rangle$ is used because a dilative plastic volumetric strain rate is assumed to be negative in this study. A simple functional form tanh is used in Eq. (26) to prescribe a maximum value of the strain-dependent effect, as was suggested by experimental data. In Eq. (26), d_1 and d_2 are model parameters whose values may vary with soil densities. It is also worth mentioning that dilatancy formulations dependent on the accumulated plastic volumetric strains have also been proposed in some previous studies (Yang et al. 2003; Dafalias and Manzari 2004).

Model Simulations

The performance of the proposed model is demonstrated through comparison with a series of cyclic simple shear tests on Fraser River sand conducted at the University of British Columbia (Sriskandakumar 2004). The test samples were prepared by the air pluviation method and were densified to relative density (D_r) of 41, 44, 80, and 81% under applied pressues (p_0') of 100 and 200 kPa, respecively. Samples were then subjected to cyclic shear for a range of cyclic stress ratios (CSRs = 0.1, 0.12, 0.3, and 0.35) under constant volume conditions that simulate the undrained response. Test data are also available on the following website: http://www.civil.ubc.ca/liquefaction/.

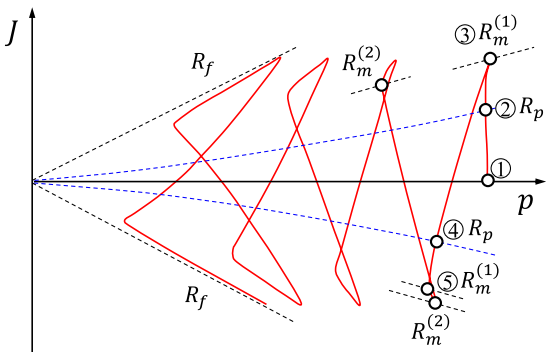

Fig. 5. Stress path using modulus formulation by Wang et al. (1990)

Summary of Model Parameters and Calibration Procedure

The model calibration and estimation procedure will be briefly discussed in this section. According to laboratory tests, Fraser River sand assumes a maximum void ratio of 0.94 and a minimum void ratio of 0.62. The grain size distribution is rather uniform, and the median grain size is $D_{50} = 0.26$ mm.

The critical state parameters (e_Γ, λ, ξ) can be estimated based on critical state test data provided by Chillarige et al. (1997). The failure line R_f can be obtained directly by fitting the maximum slope of the effective stress path in $p-J$ space. Alternatively, if the critical friction angle ϕ_f is known, $R_f = M/\sqrt{3}$, where $M = q/p = (6\sin\phi_f)/(3-\sin\phi_f)$.

The parameter κ is related to the elastic bulk modulus. κ has the same meaning as the swelling index defined in the consolidation theory for clays, but it is difficult to measure by laboratory tests for sands. Eq. (19) is then used to estimate the κ value using a drained Poisson's ratio $\nu = 0-0.1$ [$\nu = 0.05$ is used in this study following Dafalias and Manzari (2004)].

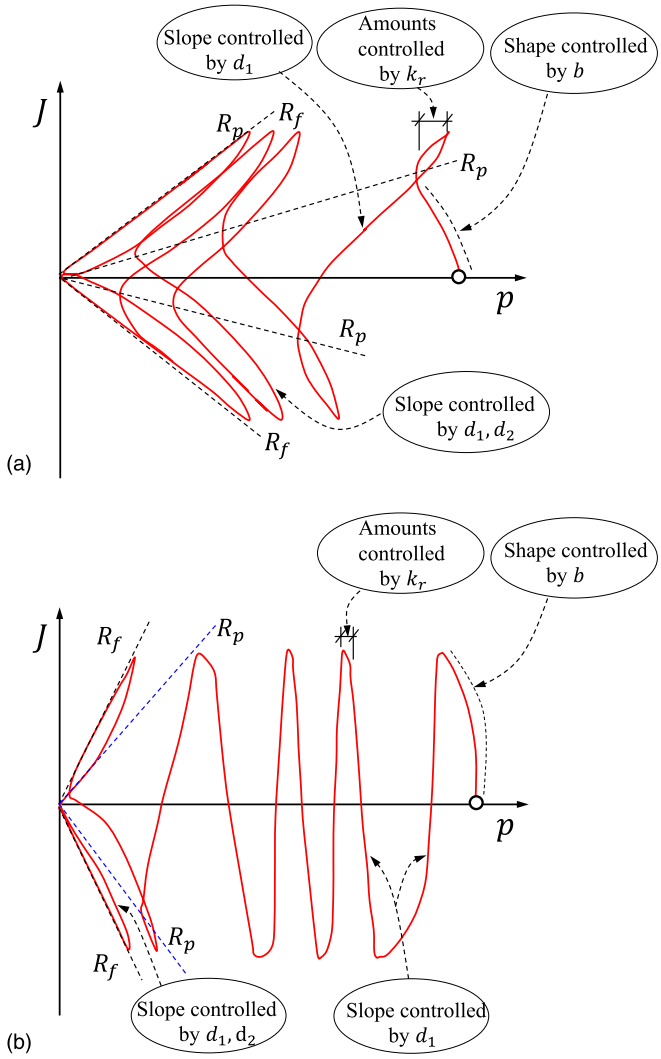

Fig. 6. Controlling parameters of the effective stress paths

J. Eng. Mech. 2014.140:91-101.

The elastic shear modulus G_{max} [denoted as G in Eq. (16)] can be determined by the following equation:

$$G_{max} = \rho V_s^2 \tag{28}$$

where ρ = soil density; and V_s = shear wave velocity. Substituting G_{max} into Eq. (16), G_0 can be back-calculated given the void ratio e and effective mean stress p. If the shear wave velocity is not available, G_{max} can be estimated by directly fitting the small-strain shear modulus from the test data.

The parameter m in Eq. (4) controls the general shape of the dilatancy line, which can be determined by fitting the phase transformation points observed in the test data. Different m values may need to be specified to model sands of different densities, as it was found in this study that using a single value of m is not appropriate for both dense and loose sands ($m = 4$ and 1.2 are specified for $D_r = 80\%$ and $D_r = 40\%$, respectively, in the following simulation). This is not a serious limitation in modeling cyclic behaviors of sands under undrained condition (i.e., the density remains constant), as is often encountered in earthquake engineering simulation. Although more thorough investigation is needed, it is recommended for practical purposes to interpolate the m value between different relative densities or express m as a function of the state parameter ψ, for a general boundary value problem where a significant change in soil density is expected.

Table 1. Summary of Model Parameters

Critical state	Phase transformation	Elastic moduli	Plastic shear modulus	Plastic bulk modulus
$e_\Gamma = 1.029$	$m = 4$	$G_0 = 208$	$h_r = 0.1$	$k_r = 0.3$
$\lambda = 0.0404$	($D_r = 81\%$)	$\nu = 0.05$	$\alpha = 1.5$	$b = 0.6$
$\xi = 0.7$	$m = 1.2$			$d_1 = 4$, $d_2 = 8$
$M = 1.33$	($D_r = 40\%$)			($D_r = 81\%$)
				$d_1 = 1.1$, $d_2 = 40$
				($D_r = 40\%$)

Because the total volumetric strain remains constant in undrained tests, i.e., $\dot{\boldsymbol{\varepsilon}}_v^e + \dot{\boldsymbol{\varepsilon}}_v^p = 0$, the following equation can be obtained via the stress-strain relationships [Eqs. (5) and (6)]:

$$\frac{1}{K_r} p\dot{\mathbf{r}} : \bar{\mathbf{n}} = -\frac{\dot{p}}{K} \tag{29}$$

Substituting $K_r = K/w$ [Eq. (23)] into Eq. (29)

$$\dot{p} = -w(p\dot{\mathbf{r}} : \bar{\mathbf{n}}) \tag{30}$$

In an undrained triaxial or cyclic simple shear test, $\mathbf{r}$, $\dot{\mathbf{r}}$, and $\bar{\mathbf{n}}$ are coaxial. $\dot{\mathbf{r}}$ is always along $\bar{\mathbf{n}}$; therefore, $\dot{\mathbf{r}} : \bar{\mathbf{n}} > 0$. However, $\bar{\mathbf{n}}$ and $\mathbf{r}$ may be of the same or opposite direction, i.e., $\text{sign}(\dot{\mathbf{r}} : \mathbf{r}) = \text{sign}(\dot{R})$.

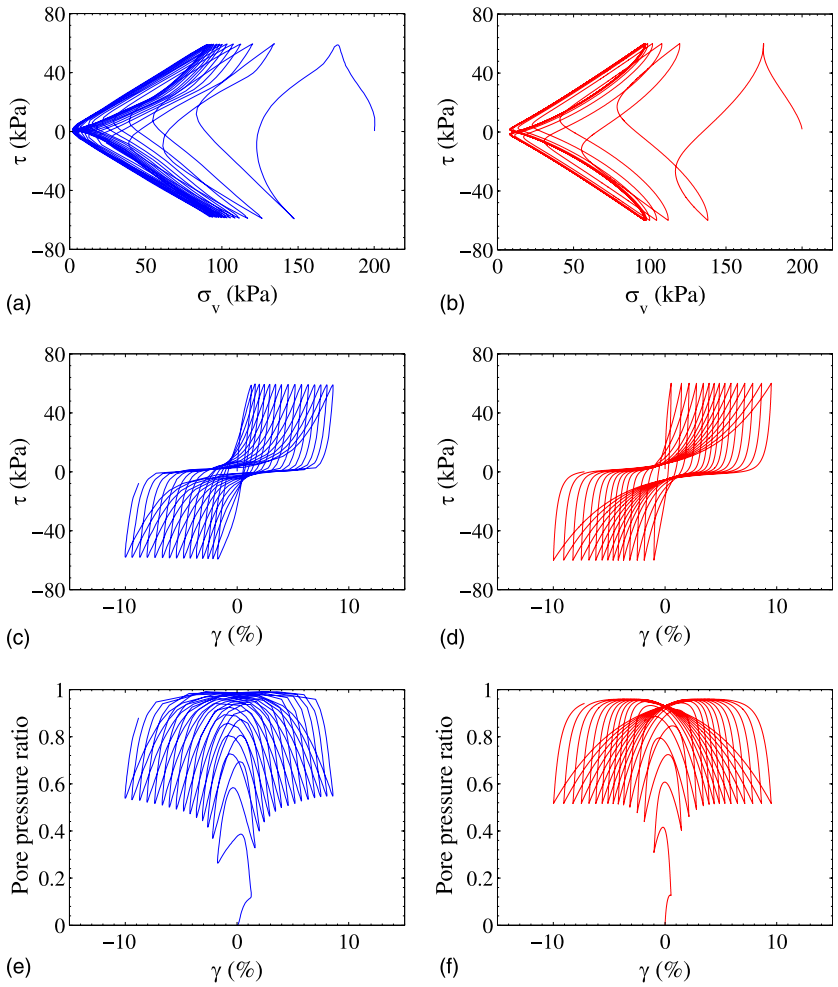

Fig. 7. Comparison of model simulation for $D_r = 81\%$, $p_0' = 200$ kPa, CSR = 0.3

J. Eng. Mech. 2014.140:91-101.

Therefore, the slope of effective stress path in $p-J$ space, dJ/dp, can be obtained as follows (Wang et al. 1990):

$$\dot{p} = -wp\left(\sqrt{2}\left|\left|\dot{R}\right|\right|\right) \tag{31}$$

$$\Rightarrow \dot{p} = -\left[\text{sign}\left(\dot{R}\right)\sqrt{2}w\right]\left(\dot{J} - \dot{p}R\right) \tag{32}$$

$$\Rightarrow \frac{dJ}{dp} = R - \frac{\text{sign}\left(\dot{R}\right)}{\sqrt{2}w} \tag{33}$$

Based on this expression, the slope of the effective stress path can be uniquely determined by R and w. In fact, parameters k_r, b, d_1, and d_2 in Eq. (25) control different parts of the effective stress path as is illustrated in Fig. 6. Accordingly, these parameters can be reasonably calibrated based on different parts of the effective stress path in an undrained cyclic shear test. In particular, k_r specifies the slope of dilative stress path in the dense sample. For the loose sample, k_r specifies the amount of contraction in the stress path when the previous maximum stress ratio is exceeded. The parameters b and d_1 control the slope of the effective stress path during the contractive phase of the virgin loading and the subsequent loading cycles, respectively. Parameter d_2 controls the rate of progressive change in the slope of the contractive stress path. Generally speaking, an increase in d_1 implies a more contractive response, i.e., a smaller slope of the contractive stress path. An increase in d_2 implies a faster rate of increase in contraction through repeated cycles.

Parameter h_r in Eq. (20) is related to the plastic shear modulus, and it affects the nonlinear shear stress-strain relationship of the soil. h_r can be calibrated against a given shear modulus reduction curve, which shows the reduction of the secant shear modulus (normalized by the elastic shear modulus) versus the strain amplitude for each loading cycle. The modulus reduction curve has been widely used to characterize the equivalent nonlinearity of the soil in a dynamic analysis.

Parameter α in Eq. (21) is mainly used to control the rate of the progressive accumulation of shear strains in cyclic mobility. The number of loading cycles needed to reach a large strain level (e.g., 5%) can be used to determine the α value. Generally, a smaller α value should be specified if a large number of loading cycles is needed to reach a specified strain level. The calibrated parameters for Fraser River sand are summarized in Table 1. These values should be considered as typical values and should be well served as the starting point to calibrate other types of sands. Different values of the dilation parameter m and plastic bulk modulus parameters d_1 and d_2 are assigned for loose and dense samples based on the test data. Although further investigation is needed to study the dependency of these parameters on soil's density, it is suggested that for practical purposes these parameters can be linearly interpolated for other densities.

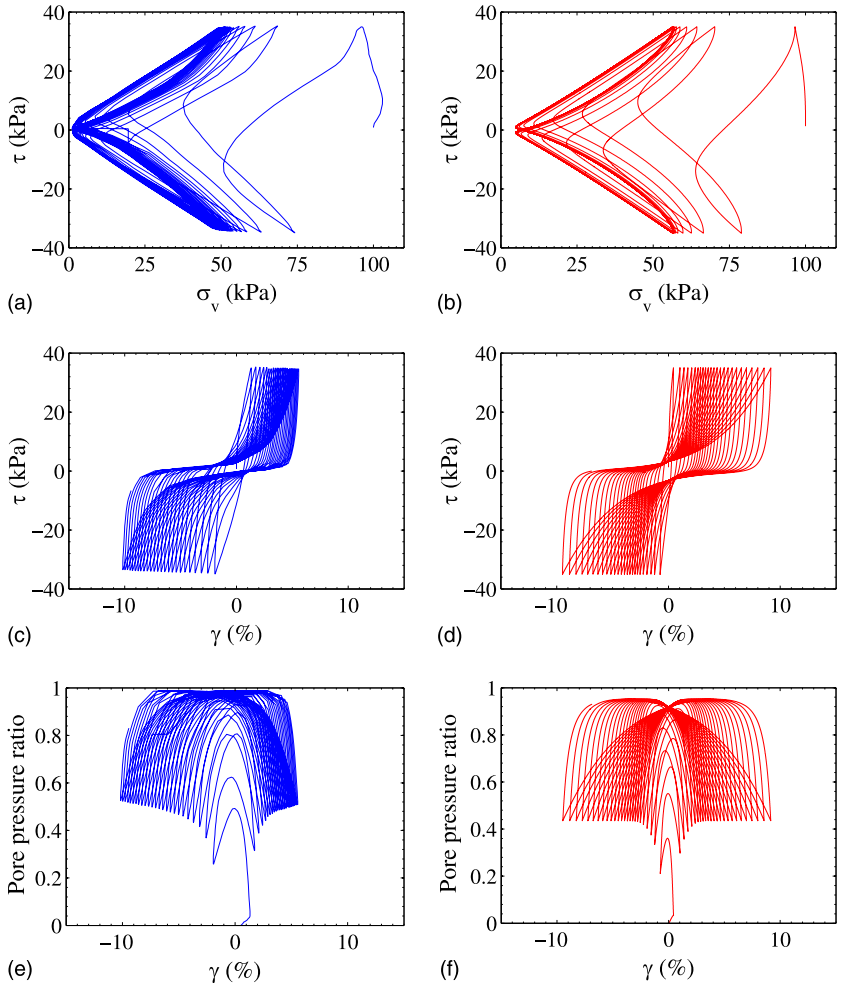

Fig. 8. Comparison of model simulation for $D_r = 80\%$, $p_0' = 100$ kPa, CSR = 0.35

J. Eng. Mech. 2014.140:91-101.

Comparison of Model Simulations

A series of undrained cyclic simple shear tests on Fraser River sand are simulated using the modified bounding surface model. Figs. 7–10 compare the effective stress path, stress-strain response, and excessive pore pressure ratio of the test results and model simulations.

During the first a few loading cycles in Figs. 7(a and b), the dense sample ($D_r = 80-81\%$) exhibits increasingly stronger contractive phases following each dilative phase. As the effective stress approaches zero, the stress path repeatedly follows a *butterfly* loop. In Figs. 7(c and d), the shear strains progressively accumulate during each loading cycle, referred to as cyclic mobility. The accumulated shear strain of both test and model simulation reaches around 10% after 15 and 25 loading cycles for two cyclic tests, respectively. The shape of the stress-strain curves also progressively change to form a *banana* pattern: as the effective stress approaches zero, small residual shear strength results in large shear strains and a flow-type mode of failure. However, during the subsequent dilative phase, considerable strain hardening and recovery of shear strength are observed. Progressive buildup of effective pore pressure ratio is also compared in Figs. 7(e and f).

On the other hand, the loose samples ($D_r = 40-44\%$) exhibit a purely contractive response and continuous reduction of effective stress during the first a few cycles in Figs. 9(a and b) and 10(a and b). Once the effective stress approaches zero, large cyclic strains suddenly develop, as shown in Figs. 9(c and d) and 10(c and d). The postliquefaction stress-strain response of the loose sand is similar to that of the dense sand where shear strength is regained through strain hardening during the dilative phase. Although the postliquefaction deformation is more difficult to capture accurately, the simulation results are in close agreement with the experimental tests such that the shear strain reaches around 16 and 10% after five and seven cycles in these two tests, respectively. Progressive buildup of effective pore pressure ratio in loose samples is also compared in Figs. 9(e and f) and 10(e and f). The proposed model demonstrated an excellent capability in simulating the effective stress paths, stress strain behaviors, and pore pressure buildup of both dense and loose soil samples.

Conclusions

Modeling undrained cyclic behaviors of sandy soils has important applications in geotechnical earthquake engineering. The bounding surface hypoplasticity model, originally proposed by Wang et al. (1990), has been widely used to simulate seismic response and liquefaction phenomena of saturated sands. However, the model was developed based on experimental data on liquefiable loose sands and is not suitable for simulating cyclic behaviors of sands in the dense state.

A modified bounding surface hypoplasticity model is developed in this study to improve the simulation of distinct dilatancy behaviors of both loose and dense sandy soils during various phases of cyclic loading. More general modulus formulations are proposed

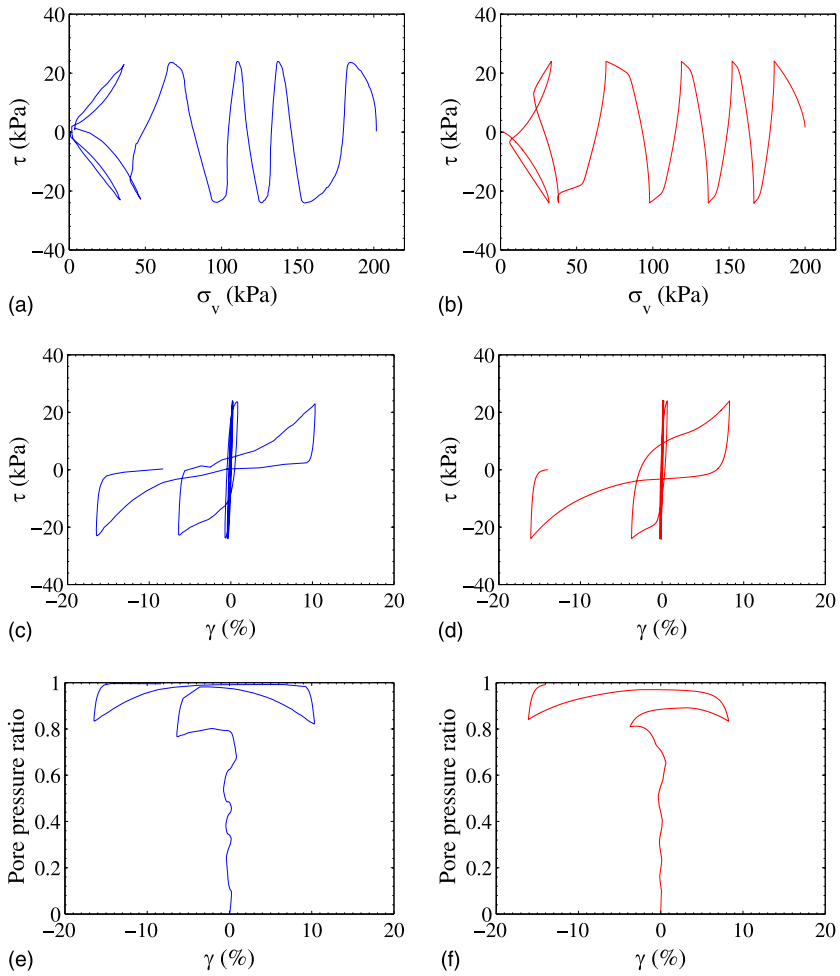

Fig. 9. Comparison of model simulation for $D_r = 44\%$, $p_0' = 200$ kPa, CSR = 0.12

J. Eng. Mech. 2014.140:91-101.

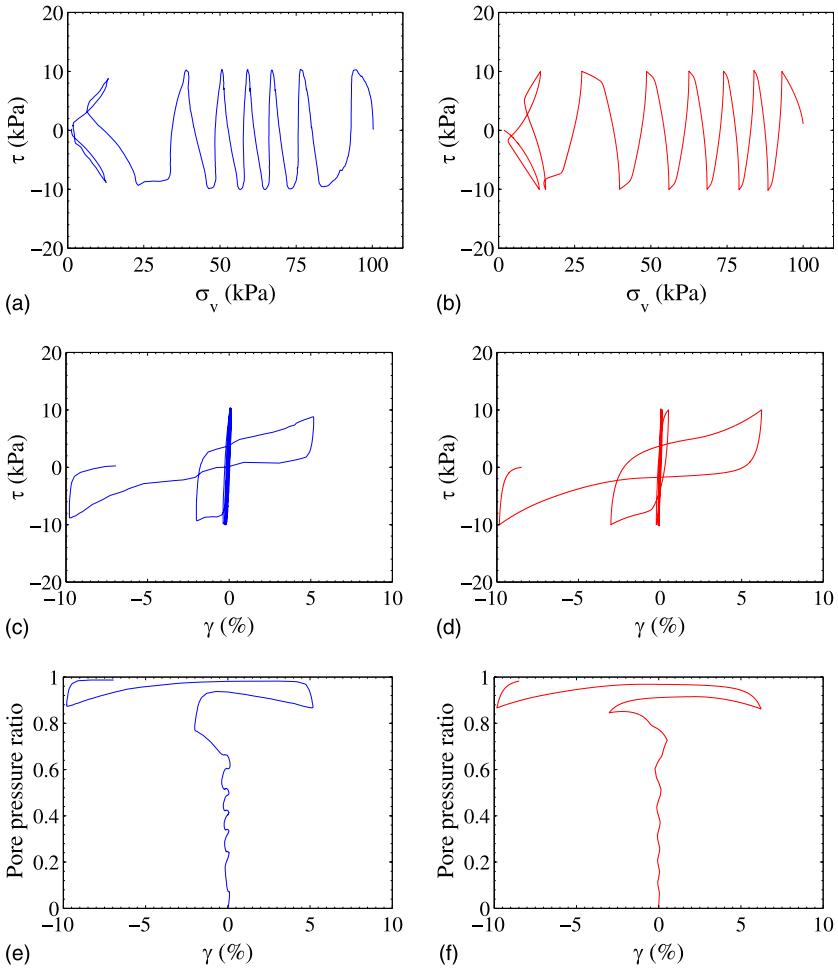

Fig. 10. Comparison of model simulation for $D_r = 40\%$, $p_0' = 100\,\text{kPa}$, CSR = 0.1

based on observation from laboratory tests and a set of new postulates. The proposed model also features a state-dependent dilatancy surface and incorporates the effects of the accumulated plastic strains on the plastic moduli to better simulate cyclic mobility and postliquefaction behaviors. Comparison of the model simulations with a set of undrained cyclic simple shear test on Fraser River sand demonstrated its excellent performance in simulating cyclic mobility and postliquefaction behavior of both loose and dense sands.

Acknowledgments

The authors thank Dr. Zhi-Liang Wang for his many insightful discussions during the course of this study. Financial support from Research Project Competition (UGC/HKUST) Grant No. RPC11EG27 and Hong Kong Research Grants Council Grant No. RGC 620311 is gratefully acknowledged.

References

Anandarajah, A. (2008). "Modeling liquefaction by a multimechanism model." *J. Geotech. Geoenviron. Eng.*, 134(7), 949–959.

Arulanandan, K., Li, X. S., and Sivathasan, K. (2000). "Numerical simulation of liquefaction-induced deformations." *J. Geotech. Geoenviron. Eng.*, 126(7), 657–666.

Been, K., and Jefferies, M. G. (1985). "A state parameter for sands." *Geotechnique*, 35(2), 99–112.

Chillarige, A. V., Robertson, P. K., Morgenstern, N. R., and Christian, H. A. (1997). "Evaluation of the in situ state of Fraser River sand." *Can. Geotech. J.*, 34(4), 510–519.

Dafalias, Y. F. (1986). "Bounding surface plasticity: I. Mathematical foundation and hypoplasticity." *J. Eng. Mech.*, 112(9), 966–987.

Dafalias, Y. F., and Manzari, M. T. (2004). "Simple plasticity sand model accounting for fabric change effect." *J. Eng. Mech.*, 130(6), 622–634.

Elgamal, A., Yang, Z., Parra, E., and Ragheb, A. (2003). "Modeling of cyclic mobility in saturated cohesionless soils." *Int. J. Plast.*, 19(6), 883–905.

Ishihara, K., Tatsuoka, F., and Yasuda, S. (1975). "Undrained deformation and liquefaction of sand under cyclic stresses." *Soils Found.*, 15(1), 29–44.

Kramer, S. (1996). *Geotechnical earthquake engineering*, Prentice Hall, Upper Saddle River, NJ.

Li, X. S. (2002). "A sand model with state-dependent dilatancy." *Geotechnique*, 52(3), 173–186.

Li, X. S., Dafalias, Y. F., and Wang, Z. L. (1999). "State-dependent dilatancy in critical-state constitutive modelling of sand." *Can. Geotech. J.*, 36(4), 599–611.

Li, X. S., Shen, C. K., and Wang, Z. L. (1998). "Fully coupled inelastic site response analysis for 1986 Lotung earthquake." *J. Geotech. Geoenviron. Eng.*, 124(7), 560–573.

Li, X. S., and Wang, Y. (1998). "Linear representation of steady-state line for sand." *J. Geotech. Geoenviron. Eng.*, 124(12), 1215–1217.

Li, X. S., Wang, Z. L., and Shen, C. K. (1992). "SUMDES: A nonlinear procedure for response analysis of horizontally-layered sites subjected to multi-directional earthquake loading." Dept. of Civil Engineering, Univ. of California, Davis, CA.

Manzari, M. T., and Dafalias, Y. F. (1997). "A critical state two-surface plasticity model for sands." *Geotechnique*, 47(2), 255–272.
Nemat-Nasser, S., and Tobita, Y. (1982). "Influence of fabric on liquefaction and densification potential of cohesionless sand." *Mech. Mater.*, 1(1), 43–62.
Park, S. S., and Byrne, P. M. (2004). "Practical constitutive model for soil liquefaction." *Proc., 9th Int. Symp. on Numerical Models in Geomechanics (NUMOG IX)*, Taylor and Francis, London, 181–186.
Pastor, M., Zienkiewicz, O. C., and Chan, A. H. C. (1990). "Generalized plasticity and the modelling of soil behaviour." *Int. J. Numer. Anal. Methods Geomech.*, 14(3), 151–190.
Prevost, J. H. (1981). "*DYNA FLOW*: A nonlinear transient finite element analysis program." *Rep. No. 81-SM-1*, Dept. of Civil Engineering, Princeton Univ., Princeton, NJ.
Sriskandakumar, S. (2004). "Cyclic loading response of Fraser River sand for validation of numerical models simulating centrifuge tests." M.S. thesis, Univ. of British Columbia, Vancouver, BC, Canada.
Taiebat, M., and Dafalias, Y. F. (2008). "SANISAND: Simple anisotropic sand plasticity model." *Int. J. Numer. Anal. Methods Geomech.*, 32(8), 915–948.
Verdugo, R., and Ishihara, K. (1996). "The steady-state of sandy soils." *Soils Found.*, 36(2), 81–91.
Wang, Z., Chang, C. Y., and Mok, C. M. (2001). "Evaluation of site response using downhole array data from a liquefied site." *Proc., 4th Int. Conf. on Recent Advances in Geotechnical Earthquake Engineering and Soil Dynamics*, S. Prakash, ed., Univ. of Missouri, Rolla, MO.
Wang, Z. L. (1990). "Bounding surface hypoplasticity model for granular soils and its applications." Ph.D. thesis, Univ. of California, Davis, CA.
Wang, Z. L., Chang, C. Y., and Chin, C. C. (2008). "Hysteretic damping correction and its effect on non-linear site response analyses." *Proc., Geotechnical Earthquake Engineering and Soil Dynamics IV*, ASCE, Reston, VA.
Wang, Z. L., and Dafalias, Y. F. (2002). "Simulation of post-liquefaction deformation of sand." *Proc., 15th ASCE Engineering Mechancis Conf.*, ASCE, Reston, VA.
Wang, Z. L., Dafalias, Y. F., Li, X. S., and Makdisi, F. I. (2002). "State pressure index for modeling sand behavior." *J. Geotech. Geoenviron. Eng.*, 128(6), 511–519.
Wang, Z. L., Dafalias, Y. F., and Shen, C. K. (1990). "Bounding surface hypoplasticity model for sand." *J. Eng. Mech.*, 116(5), 983–1001.
Wang, Z. L., and Makdisi, F. I. (1999). "Implementation a bounding surface hypoplasticity model for sand into the *FLAC* program." *FLAC and numerical modeling in geomechanics*, Balkema, Rotterdam, Netherlands, 483–490.
Wang, Z. L., Makdisi, F. I., and Egan, J. (2006). "Practical applications of a nonlinear approach to analysis of earthquake-induced liquefaction and deformation of earth structures." *Soil. Dyn. Earthquake Eng.*, 26(2–4), 231–252.
Yang, Z. H., Elgamal, A., and Parra, E. (2003). "Computational model for cyclic mobility and associated shear deformation." *J. Geotech. Geoenviron. Eng.*, 129(12), 1119–1127.
Yin, Z. Y. and Chang, C. (2013). "Stress-dilatancy behavior for sand under loading and unloading conditions." *Int. J. Numer. Anal. Meth. Geomech.*, 37(8), 855–870.
Yin, Z. Y., Chang, C., and Hicher, P. (2010). "Micromechanical modelling for effect of inherent anisotropy on cyclic behaviour of sand." *Int. J. Solids Struct.*, 47(14–15), 1933–1951.
Zienkiewicz, O. C., Chan, A. H. C., Pastor, M., Schrefler, B. A., and Shiomi, T. (1999). *Computational geomechanics: With special reference to earthquake engineering*, Wiley, New York.